Science Bulletin 64 (2019) 856–864

Contents lists available at ScienceDirect

Science Bulletin

journal homepage: www.elsevier.com/locate/scib

Article

Single-phase high-entropy intermetallic compounds (HEICs): bridging high-entropy alloys and ceramics

Naixie Zhou [a,b], Sicong Jiang [a], Timothy Huang [a], Mingde Qin [a], Tao Hu [c,a,*], Jian Luo [a,*]

[a] Department of Nanoengineering, Program of Materials Science and Engineering, University of California, San Diego, CA 92093-0448, USA
[b] Oerlikon Metco Inc., San Diego, CA 92121, USA
[c] State Key Laboratory of High Performance and Complex Manufacturing, School of Materials Science and Engineering, Central South University, Changsha 410083, China

ARTICLE INFO

Article history:
Received 27 February 2019
Received in revised form 13 April 2019
Accepted 7 May 2019
Available online 13 May 2019

Keywords:
High-entropy intermetallic compound
Aluminide
Phase stability
High-entropy alloy
High-entropy ceramic

ABSTRACT

High-entropy intermetallic compounds (HEICs) were fabricated by mechanical alloying and spark plasma sintering to fill a knowledge gap between the traditional high-entropy alloys (HEAs) and emerging high-entropy ceramics (HECs). Notably, several four- or five-component equimolar aluminides, such as the B2-phase $(Fe_{1/5}Co_{1/5}Ni_{1/5}Mn_{1/5}Cu_{1/5})Al$, have been made into single-phase HEICs for the first time. Thermodynamic modeling and a reversible, temperature-dependent, phase-stability experiment suggest that such B2-phase HEICs are entropy-stabilized phases. The structure of these HEICs resembles that of HECs with high-entropy mixing of four or five elements of nearly equal fractions in one and only one sublattice, but with significant (~10%) anti-site defects (differing from typical HECs). A new phase stability rule for forming single B2-phase HEICs is proposed. Five additional HEICs of predominantly DO_{22} phases have also been made. This study broadens the families of equimolar, single-phase, high-entropy materials that have been successfully fabricated.

© 2019 Science China Press. Published by Elsevier B.V. and Science China Press. All rights reserved.

1. Introduction

High-entropy alloys (HEAs) consisted of at least four principal metallic elements with near equimolar fractions, also known as "multi-principal element alloys (MPEAs)" or "complex concentrated alloys (CCAs)", have attracted significant research interests in last 15 years [1–8]. Compared with traditional alloys with one primary element and several minor alloying dopants, HEAs explore new compositional spaces where no single component is dominant. Examples of HEAs include the famous face-centered cubic (FCC) "Cantor alloy" CoCrFeMnNi [8] and refractory body-centered cubic (BCC) HEAs (e.g., TaMoNbVW) [3,4]. HEAs can often possess excellent mechanical physical properties, e.g., high strength and ductility [1,2,6,7,9–11], high fracture toughness [12], irradiation resistance [13,14], fatigue resistance [15], corrosion resistance [16,17], and excellent cryogenic or high-temperature performance [4,5]. In particular, Al-containing HEAs have been studied, where Al can affect the microstructures and mechanical behavior of HEAs [18–20].

On the one hand, prior studies of metallic HEAs focus on simple solid solution phases where the multiple principal elements randomly occupy the same type lattice site of the FCC, BCC or hexagonal close packed (HCP) structure. On the other hand, an increasing number of new high-entropy ceramics (HECs) have been made in the last four years [21–31], where multiple principal metal cations occupy one sublattice, with another ordered anion sublattice with little or no mixing. Examples of single-phase HECs that have been successfully fabricated in last a few years include rocksalt oxides (e.g., $(Mg_{0.2}Co_{0.2}Ni_{0.2}Cu_{0.2}Zn_{0.2}O)$ [21,32], metal diborides (e.g., $(Hf_{0.2}Zr_{0.2}Ta_{0.2}Nb_{0.2}Ti_{0.2})B_2$) [22], fluorite oxides (e.g., $(Hf_{0.2}Zr_{0.2}Ce_{0.2}Y_{0.2}Gd_{0.2})O_{2-\delta}$) [24], perovskites (e.g., $(Ba_{0.5}Sr_{0.5})(Zr_{0.2}Sn_{0.2}Ti_{0.2}Hf_{0.2}Nb_{0.2})O_3$) [23], carbides (e.g., $(Hf_{0.2}Zr_{0.2}Ta_{0.2}Nb_{0.2}Ti_{0.2})C$) [27–30], and silicides (e.g., $(Mo_{0.2}Nb_{0.2}Ta_{0.2}Ti_{0.2}W_{0.2})Si_2$) [31]. These HECs also possess some unique or superior properties, such as reduced low thermal conductivities [28,32] and increased hardness [27–30,33].

This study further fills a knowledge gap between the traditional (metallic) HEAs and the emerging (mostly ionic) HECs via fabricating a new class of single-phase high-entropy intermetallic compounds (HEICs), exemplified by equimolar high-entropy aluminides such as the B2-phase $(Fe_{1/5}Co_{1/5}Ni_{1/5}Mn_{1/5}Cu_{1/5})Al$. These new HEICs are mostly metallic (albeit some mixed ionic-metallic bonds due to the different electronegativities) but have crystal structures resembling (mostly ionic) HECs: i.e., random mixing of four or five elements of equal molar fractions on one and only sublattice with another ordered sublattice with little mixing (albeit ~10% anti-site defects that are substantially higher than that in typical HECs). Thus, this discovery expands the families of

* Corresponding authors.
E-mail addresses: tao.hu@csu.edu.cn (T. Hu), jluo@alum.mit.edu (J. Luo).

https://doi.org/10.1016/j.scib.2019.05.007
2095-9273/© 2019 Science China Press. Published by Elsevier B.V. and Science China Press. All rights reserved.

single-phase, equimolar, high-entropy materials that have been successfully fabricated to date, and it bridges HEAs and HECs.

While the fabrication of single-phase HEICs has not been reported before, we recognize that multicomponent intermetallic compounds have been observed widely in complex alloys including HEAs as secondary phases [6,34–38]. Notably, Lu et al. [34] reported an eutectic HEA, $AlCoCrFeNi_{2.1}$, and attributed the two phases as FCC and (ordered BCC-based) B2 based on X-ray diffraction (XRD). A follow-up study on the same $AlCoCrFeNi_{2.1}$ HEA by Nagase et al. [35], however, suggested the formation of the ordered (FCC-based) $L1_2$ in the dendritic region, along with disordered FCC and BCC in the eutectic region, by using more sensitive electron diffraction. Furthermore, four eutectic HEAs ($CoCrFeNiM_{0.45}$, where M= Nb, Ta, Zr, or Hf) with FCC and Laves phases were designed and fabricated via casting [36]. These Laves phases are enriched in two or three elements (thereby being far away from equimolar compositions) [36]. CALPHAD (calculation of phase diagram) modeling also suggested the existence of FCC-B2 two-phase regions in several HEAs [39]. Zhao and co-workers [26] recently investigated three $Al_xCo_{0.2}Cr_{0.2}Ni_{0.2}Ti_{0.4-x}$ multi-phase HEAs with substantial amounts of multicomponent B2 phases that presumably have three principal elements (Co, Cr, and Ni) on one sublattice and another two (Al and Ti) primarily on the other sublattice; this represents one reported case that is perhaps the most close to (but not yet truly) HEICs, and none of them is single-phase. To the best of our knowledge, none of these prior studies aimed at fabricating and investigating single-phase HEICs. Interestingly, two recent studies by Yang et al. [6] and He et al. [37] used multicomponent intermetallic nanoparticles (MCINPs) of the $L1_2$ [6] and $D0_{22}$ [37] structure, in the form of nanoscale precipitates in the continuous matrix of complex alloys [6] or HEAs [37], to strengthen the FCC-based alloys. Here, these MCINPs, e.g., $(Ni_{35}Co_{17}Fe_8)(Al_7Ti_{11}Co_2)$ $L1_2$ (resemble Ni_3Ti or Ni_3Al) [6] and $Ni_{65.2}Nb_{24.1}Co_{7.7}Cr_{1.4}Fe_{1.3}$ $D0_{22}$ (close to Ni_3Nb) phases, are enriched in only one, or at most two, principal element(s) in each sublattice (so they are not multi-principal element high-entropy phases), and they are not the primary phases. Thus, the current study aims to make the first research effort to fabricate and subsequently characterize and investigate single-phase HEICs.

To seek the existence of single-phase HEICs with random mixing of four or five elements of a nominally equimolar fraction on one and only one sublattice (resembling HECs), we selected B2 phase high-entropy aluminides as our primary model systems. In addition, we further explored $D0_{22}$-phase high-entropy aluminides as a second structure to extend generality of this study. Aluminides were chosen in this study because they are important structural materials for their light weight, excellent thermal stability, outstanding oxidation resistance, and high strength [40]. The B2 phase is an ordered BCC-based structure, i.e., the CsCl type structure albeit significant anti-site defects. Fig. 1a shows the schematic structure of a B2-phase high-entropy aluminide, in which four or five elements of equimolar fractions are randomly mixed on only one sublattice and Al atoms primarily occupy the other sublattice. In this study, we fabricated seven equimolar B2-phase high-entropy aluminides, including three with single (and others with predominant one) ordered B2 phases. We also showed that these B2-phase HEICs are likely entropy-stabilized phases, and we further proposed a new selection criterion for forming single-phase B2 high-entropy aluminides (as a new phase stability rule). Furthermore, we successfully fabricated five additional high-entropy aluminides of primarily $D0_{22}$ phases (with the structure illustrated in Fig. 1b) to extend the generality of this study and our discovery.

2. Materials and methods

To prepare the B2-phase high-entropy aluminides, we designed seven equal-aluminide-molar compositions (as listed in Table 1). Each non-Al element has equal molar fraction and the total molar fraction of these elements is 50% to maintain the stoichiometry of aluminide. The elements were selected based on the phase stability of binary aluminides as well as their mutual solubility. All selected specimens contain Fe, Co and Ni because AlFe, AlCo and AlNi are stable binary aluminides with pronounced mutual miscibility and close lattice constants [41,42]. Other transition metal elements, e.g., Mn, Cu and Cr, were also added into the matrix. In addition, 50% of the Al atoms were replaced with Ti in specimens #6 and #7 to further perturbate the B2 structure and extend the work beyond pure aluminides.

High-purity powders Al (99.9%), Ti (99.5%), Cr (99.95%), Fe (99.9%), Co (99.8%), Ni (99.9%), Cu (99.9%) and Mn (99.95%) purchased from Alfa Aesar (USA) were utilized as starting materials. Appropriate amounts of each powder according to the stoichiometry were used to fabricate specimens. The seven compositions for forming B2-phase HEICs are listed in Table 1 and referred to as specimen #1 to #7 in the text. The raw powders were mechanically alloyed via high energy ball milling (HEBM) using a SPEX 8000D miller (SpexCertPrep, USA) for 3 h. To prevent overheating, the

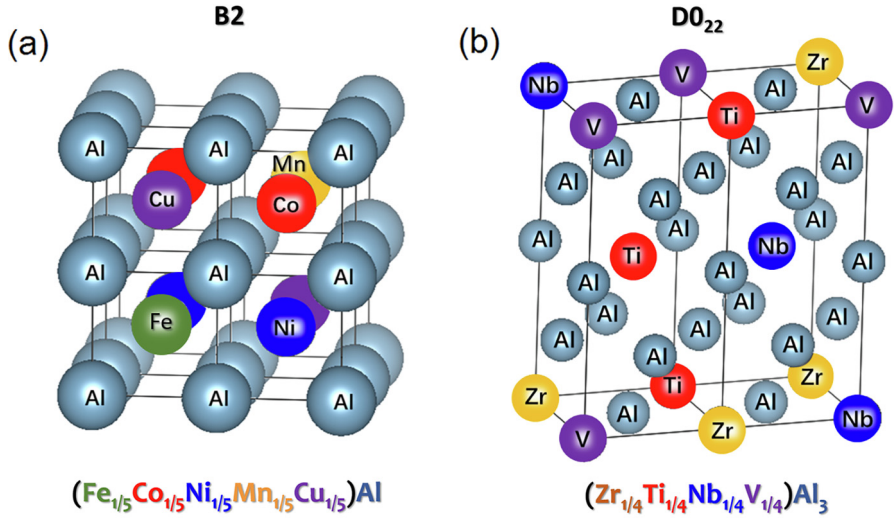

Fig. 1. (Color online) Schematic illustrations of the high-entropy aluminides with the (a) B2 and (b) $D0_{22}$ structures.

Table 1
Summary of the seven specimens that exhibit primarily or completely single high-entropy B2 phase after equilibration at 1,100 °C for 10 h.

	Composition	Is single B2 phase at 1,100 °C?	Lattice constant (Å)	δ	ΔH_{mix}	VEC	δ^*	ΔH^*_{mix}
#1	$(Fe_{1/4}Co_{1/4}Ni_{1/4}Cr_{1/4})Al$	No	2.887	7.64	−16.44	2.83	1.30	−15.50
#2	$(Fe_{1/4}Co_{1/4}Ni_{1/4}Mn_{1/4})Al$	Almost	2.895	7.78	−18.75	2.86	0.66	−17.75
#3	$(Fe_{1/4}Co_{1/4}Ni_{1/4}Cu_{1/4})Al$	Yes	2.918	7.72	−12.00	3.34	0.97	−13.25
#4	$(Fe_{1/5}Co_{1/5}Ni_{1/5}Mn_{1/5}Cr_{1/5})Al$	No	2.909	7.57	−17.24	2.69	1.18	−16.20
#5	$(Fe_{1/5}Co_{1/5}Ni_{1/5}Mn_{1/5}Cu_{1/5})Al$	Yes	2.916	7.64	−13.96	3.16	0.92	−14.40
#6	$(Fe_{1/4}Co_{1/4}Ni_{1/4}Cu_{1/4})(Al_{1/2}Ti_{1/2})$	No	2.948	7.12	−24.00	3.12	–	–
#7	$(Fe_{1/4}Co_{1/4}Ni_{1/4}Mn_{1/4})(Al_{1/2}Ti_{1/2})$	No	2.945	7.20	−28.38	2.65	–	–

HEBM was stopped every 60 min to allow cooling for 5 min. The powders were then compacted into disks of 20-mm diameter and consolidated by using spark plasma sintering (SPS, Thermal Technologies, USA).

All the consolidated bulk samples were further homogenized at 1,100 °C for 10 h in a tube furnace. The chamber was purged with a mixed gas of Ar and 5 vol% H_2. A constant flow of the gaseous mixture was maintained throughout the heat treatment. The chamber pressure is one atmosphere. The samples were air quenched and the initial cooling rate is estimated to be about 40–50 °C/min. The phase composition and lattice parameters were determined by using X-ray diffractometer (D/Max B Geigerflex, Rigaku, Japan) with Cu Kα radiation, of which the wavelength is 1.54056 Å. The compositions of the specimens were characterized by scanning electron microscopy (SEM, Quanta FEG 250, FEI, USA) equipped with energy dispersive X-ray spectroscopy (EDXS). Specifically, EDXS mapping was employed to image the size and distribution of the fine precipitates.

To test the reversible temperature-dependent stability of the B2-phase, $(Co_{1/4}Fe_{1/4}Ni_{1/4}Cu_{1/4})Al$ was chosen and annealed at 1,000, 1,100, and 1,300 °C, respectively, for 10 h, in a sequence. Subsequently, the same specimen (after equilibrated at the higher temperature of 1,300 °C) was annealed again at the lower temperature 1,000 °C isothermally for 10 h. After each annealing step, the specimen was cooled down and XRD measurement was performed to determine the reversible temperature-dependence of the phase stability.

To extend the generality of this study, five additional compositions (with 75% Al and equal molar amounts of four other transition metal elements) were selected to fabricate $D0_{22}$-phase HEICs via the same mechanical alloying and SPS procedure, followed by annealing at 1,300 °C.

3. Results and discussion

3.1. The formation of high-entropy B2 phases

The phase formation of the seven specimens equilibrated at 1,100 °C was determined by XRD patterns, as shown in Fig. 2a. For comparison, the diffraction peaks for the pure BCC (Fe as an example) and B2 structured aluminide (FeAl as an example) were also simulated. It is noted that the B2 phase (a BCC-based structure with CsCl ordering) has BCC-like diffraction peaks of (1 1 0), (2 0 0) and (2 1 1), which are indicated by dots in Fig. 2. However, the formation of ordered B2 phase is characterized by the "superlattice" diffraction peaks, (1 0 0), (1 1 1) and (2 1 0), as indicated by stars, which are "forbidden reflections" in the disordered BCC structure due to the symmetry. XRD patterns of specimens #1 to #5 match well with the B2 phase (with virtually no detectable secondary phases), indicating the successful synthesis of the B2-phase high-entropy aluminides (as one type of HEICs).

For the two Ti-contained specimens #6 $(Fe_{1/4}Co_{1/4}Ni_{1/4}Cu_{1/4})(Al_{1/2}Ti_{1/2})$ and #7 $(Fe_{1/4}Co_{1/4}Ni_{1/4}Mn_{1/4})(Al_{1/2}Ti_{1/2})$, XRD patterns showed the formation of very small amounts of secondary precipitate phases.

Derived from the XRD patterns, the lattice parameter obtained for the B2 structure for the specimens #1 to #5 is close to 2.89 Å (within 0.7% variations), as shown in Table 1. The measured lattice parameters for specimens #6 $(Fe_{1/4}Co_{1/4}Ni_{1/4}Cu_{1/4})(Al_{1/2}Ti_{1/2})$ and #7 $(Fe_{1/4}Co_{1/4}Ni_{1/4}Mn_{1/4})(Al_{1/2}Ti_{1/2})$, in which 50% Al atoms were replaced by Ti atoms (with a 15% larger atomic radius), are increased to around 2.95 Å.

3.2. Anti-site defects in B2 HEICs

Anti-site defects are commonly present in the intermetallic compounds at finite temperatures due to an entropic effect [43]. In a conventional B2 intermetallic compound AB, four possible types of substitutional point defects (anti-site A and B atoms, as well as two types of vacancies in two sublattices) can exist [43], and there are more compositional variables of the anti-site defects in HEICs.

Using the single-phase specimen #3 $(Co_{1/4}Fe_{1/4}Ni_{1/4}Cu_{1/4})Al$ as an example, we simulated a series of XRD patterns to estimate the anti-site occupation assuming, for simplicity, equimolar transition metal anti-site defects in the Al sublattice and ignoring vacancies. The modeled relative intensity of the (1 0 0) superlattice peak (normalized to the strongest (1 1 0) peak) vs. anti-site occupation fraction is plotted in Fig. 2c. The anti-site defects were then estimated to be ~10% by comparing the measured relative intensities with the simulation results. Other specimens (#1, #2, #3, #4, and #5) are estimated to have similar levels of anti-site defects at 1,100 °C.

We recognized that the grain size, residual stress, and defects can affect the intensity of the XRD peak. To reduce such effects, the samples for XRD measurements in this study were annealed at high temperature (above 1,000 °C) allowing grain growth and thermal relaxation to reduce defects and residual stress, and we found no significant texture. We also recognized that temperature can influence the fraction of anti-site effects.

3.3. Compositional homogeneity and single-phase HEICs

To examine the compositional homogeneity, SEM and EDXS were performed. The EDXS elemental mapping showed that the specimens #3 $(Co_{1/4}Fe_{1/4}Ni_{1/4}Cu_{1/4})Al$ and #5 $(Co_{1/5}Fe_{1/5}Ni_{1/5}Mn_{1/5}Cu_{1/5})Al$ are compositionally homogeneous without any detectable secondary phase.

However, Cr-enriched regions in specimens #1 $(Co_{1/4}Fe_{1/4}Ni_{1/4}Cr_{1/4})Al$ and #4 $(Co_{1/5}Fe_{1/5}Ni_{1/5}Mn_{1/5}Cr_{1/5})Al$ were revealed by EDXS mapping, despite they both appear to be single phases in XRD. EDXS mapping also suggests that specimen #2 $(Co_{1/4}Fe_{1/4}Ni_{1/4}Mn_{1/4})Al$ has very small amount of Mn-enriched precipitates. In additional, EDXS showed that specimen #6 $(Co_{1/4}Fe_{1/4}Ni_{1/4}Cu_{1/4})(Al_{1/2}Ti_{1/2})$ had Cu-enriched precipitates, and

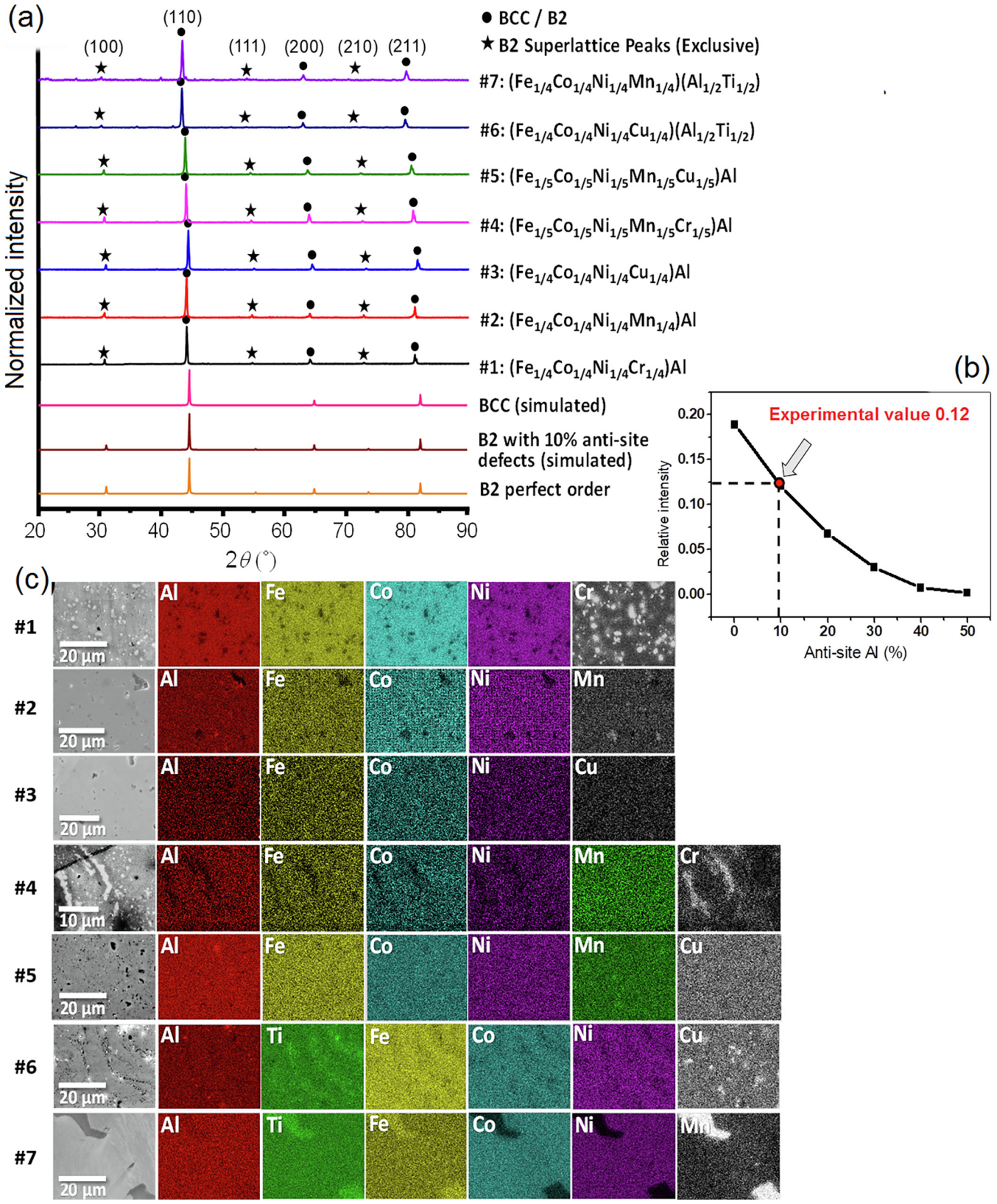

Fig. 2. (Color online) Phase constituents, elements distribution and anti-site defects in HEICs. (a) XRD patterns for seven HEIC specimens that exhibit primarily or completely single high-entropy B2 phases after annealing at 1,100 °C for 10 h. Simulated XRD peaks for the BCC (using Fe as an example), perfectly-ordered B2 (using binary FeAl as an example), and B2 phase with 10% anti-site defects are also included. Peaks that can belong to either BCC or B2 structure are indexed by dots; superlattice peaks belong exclusively to the B2 structure are indexed by stars. Minor peaks are evident in several patterns, e.g., for specimen #6 and #7, which indicate the presence of secondary phases. (b) SEM micrographs and corresponding EDXS compositional maps for specimens after annealing at 1,100 °C for 10 h. HEIC specimen #3 and #5 appear to be completely homogeneous, while specimen #2 were almost homogeneous. (c) Simulated intensity for (0 0 1) peak (normalized to the strongest (1 1 0) peak) in B2-structured aluminide as a function of the fraction of anti-site Al defects. Calculation was performed by using VESTA software.

specimen #7 ($Fe_{1/4}Co_{1/4}Ni_{1/4}Mn_{1/4}$)($Al_{1/2}Ti_{1/2}$) contained a secondary phase enriched with Ti, Fe, and Mn.

In summary, the combination of XRD and EDXS compositional mapping (Fig. 2) showed that specimens #3 ($Co_{1/4}Fe_{1/4}Ni_{1/4}Cu_{1/4}$)Al and #5 ($Co_{1/5}Fe_{1/5}Ni_{1/5}Mn_{1/5}Cu_{1/5}$)Al indeed exhibit single, high-entropy B2 phases that are compositionally homogenous. The other five specimens consist of primarily single high-entropy B2 phases, while small amounts of secondary phases or inhomogeneous regions exist; specifically, specimens #1, #2, and #4 appear to be single B2-phase HEICs in XRD patterns while EDXS mapping revealed compositional inhomogeneity.

3.4. CALPHAD modeling

We further conducted CALPHAD modeling to assess the predicted phase fraction vs. temperature curves from the ThermoCalc TCHEA database for these seven specimens (Fig. 3). While we recognize none of the current databases have been validated for HEICs (as this is the first experimental study to synthesize single B2-phase high-entropy aluminides), some useful trends can be still obtained, albeit not completely accurate, from the existing databases such as the TCHEA based on the extrapolation from the binary and ternary systems.

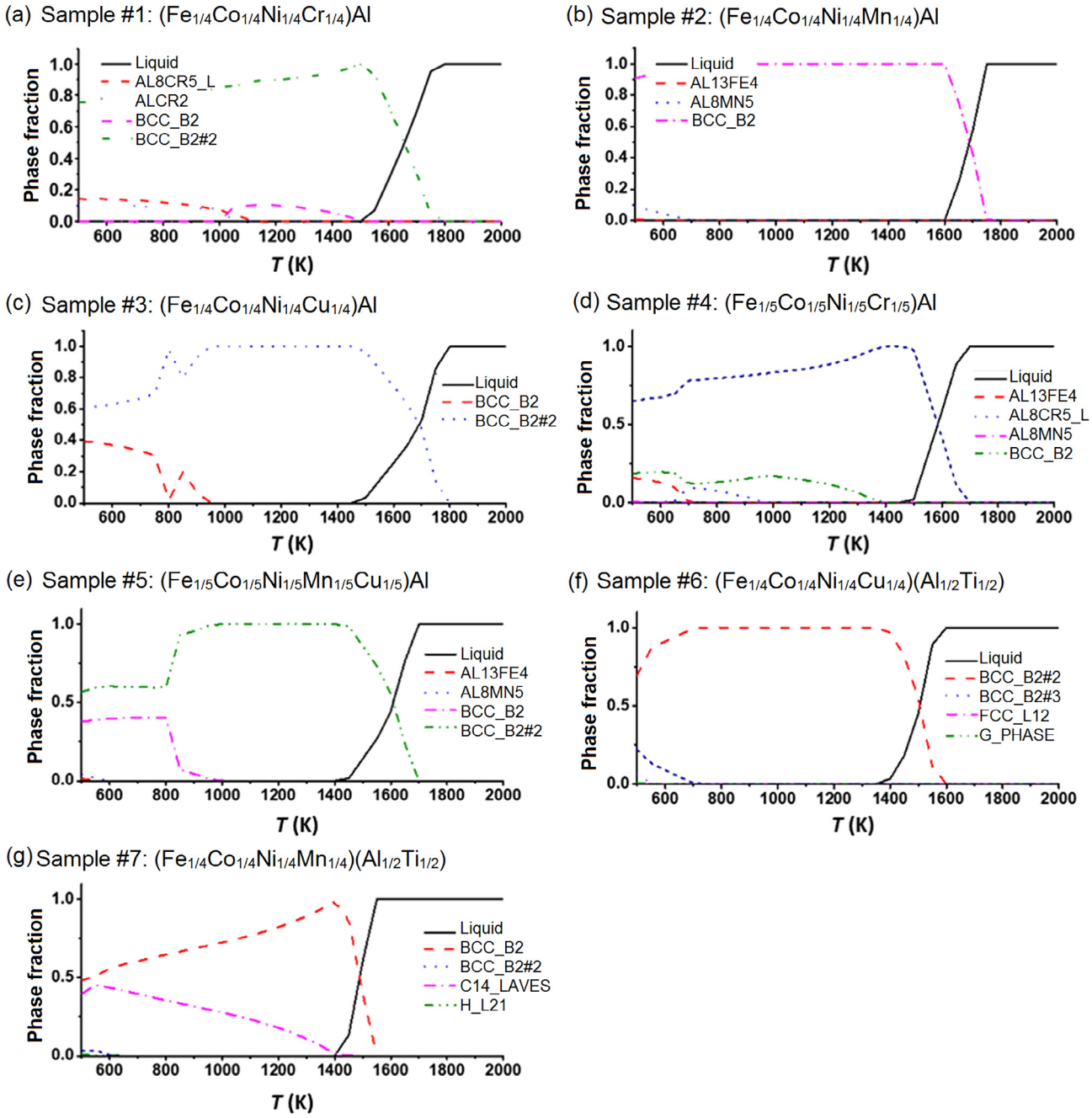

Fig. 3. (Color online) Phase evolution (volume fraction of various phases vs. equilibrium temperature) predicted by ThermoCalc using TCHEA database. The CALPHAD can be used to forecast some general trends (to the first order of approximation), but the predictions are not all accurate when they are compared with Figs. 2 and 4. This is presumably due to that the database does not include all interactions in aluminides. (a)–(g) Samples #1–#7.

The CALPHAD results showed that the primary phase at high temperatures (around 1,100 °C) is ordered B2 phase for all samples. Among them, the B2 phase fractions of the specimens #2, #3 and #5 are high (nearly 100%) in the temperature range of 1,000–1,400 K, which are consistent with experiments. The CALPHAD results also indicated that both specimens #1 and #4 should contain a Cr-rich secondary BCC phase (with ~55% Cr, ~15% Fe and ~25% Al) and a Fe-Mn-Ti-enriched Laves phase should precipitate in specimen #7, which all agree with the EDXS elemental maps (Fig. 3c).

However, the CALPHAD modeling failed to predict the precipitation of the secondary phase in specimen #6, as observed in the experiment. Moreover, CALPHAD predict a single B2 phase from 700 K to the solidus temperature ~1,600 K for specimen #2, but we observed a reversible secondary phase formation at 1,100 °C or lower (Fig. 4). It is not surprising that CALPHAD modeling is not completely accurate, since this current study represents the first experimental effort to synthesize single B2-phase high-entropy aluminides. Thus, all current databases are likely extrapolation from the partial data of binary and ternary aluminides without direct confirmation and calibration of the high-entropy B2-phase stability.

3.5. Entropy-stabilized phases

Although the CALPHAD predictions (presumably extrapolated from the data of binary and ternary aluminides) are not completely accurate, they (with extrapolation from the binary and ternary data) are able to show an important (and valid) general trend (Fig. 4): i.e., the equimolar, single high-entropy B2 phases are generally stable at high temperatures (just below the solidus temperatures), while some secondary phases precipitate at lower temperatures. This general trend suggests that these B2-phase HEICs are entropy-stabilized.

To more critically assess this hypothesis of entropy stabilization, specimen #2 ($Co_{1/4}Fe_{1/4}Ni_{1/4}Mn_{1/4}$)Al was selected to study the reversible temperature stability of the high-entropy B2 phase. The XRD patterns in Fig. 4 showed that specimen #2 exhibited two phases, the primary B2 phase and a secondary phase indicated by solid triangles, when equilibrated at 1,000 °C. The amount of the secondary phase reduced after further annealing at 1,100 °C, and the secondary phase vanished (dissolved completely into the B2 matrix) at 1,300 °C to form a single high-entropy B2 phase. Interestingly, when the same sample was isothermally annealed again at 1,000 °C after forming single high-entropy B2 phase at 1,300 °C, the secondary phase emerged again. The EDXS maps shown in Fig. 4b further confirmed the precipitation at 1,000 °C, and the dissolution of the precipitates at 1,300 °C. Specifically, the precipitates are a Mn-rich phase with composition close to 50% Mn, 25% Al, 15% Fe, 5% Co, and 5% Ni.

Similar reversible precipitation of a CuO-enriched secondary phase at low temperatures in ($Mg_{0.2}Co_{0.2}Ni_{0.2}Cu_{0.2}Zn_{0.2}$)O was reported previously and considered as the main evidence of forming this entropy-stabilized oxide [21]. Thus, Fig. 4 also implies that

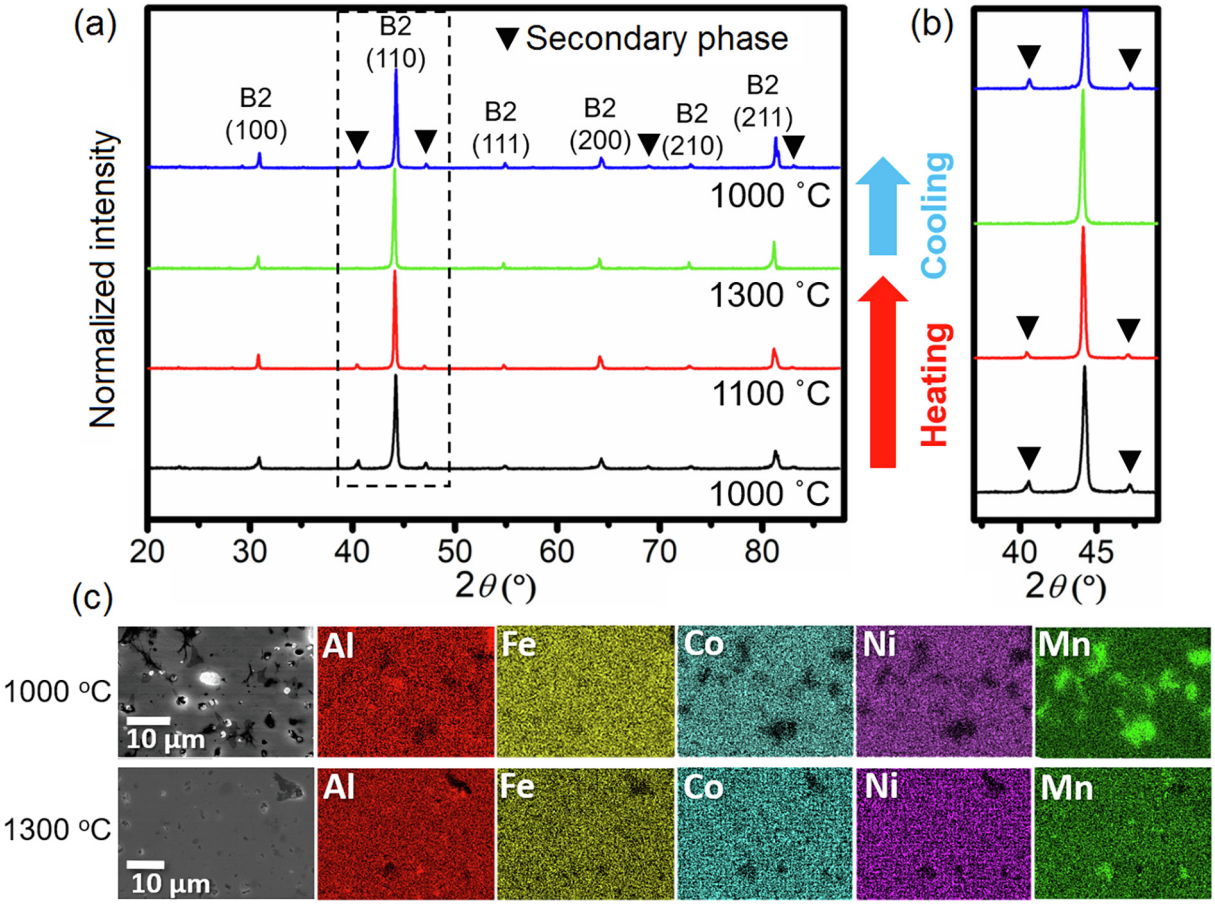

Fig. 4. (Color online) Verification of phase stability. (a) XRD patterns of the same #2 ($Fe_{1/4}Co_{1/4}Ni_{1/4}Mn_{1/4}$)Al specimen annealed at 1,000, 1,100, 1,300, and 1,000 °C sequentially (each for 10 h). (b) The enlarged XRD peaks showing the evolution of the secondary phase. (c) EDXS mapping of the same specimen annealed at 1,300 and 1,100 °C, respectively. The secondary phase that formed at 1,000 and 1,100 °C vanished after annealing at high temperature of 1,300 °C, but re-precipitated after subsequent re-annealing at 1,000 °C. This model experiment implies that the single B2 solid-solution phase is likely entropy-stabilized at high temperatures (and the CALPHAD prediction from the TCHEA database shown in Fig. 3b is not all accurate).

this single-phase equimolar HEIC observed in this study is likely entropy-stabilized at high temperatures.

It is also interesting to note that while specimen #5 ($Co_{1/5}Fe_{1/5}Ni_{1/5}Mn_{1/5}Cu_{1/5}$)Al exhibits a single high-entropy B2 phase at 1,100 °C, six out of the ten equimolar ternary aluminide subsystems, i.e., ($Co_{1/2}Ni_{1/2}$)Al, ($Cu_{1/2}Co_{1/2}$)Al, ($Mn_{1/2}Cu_{1/2}$)Al, ($Fe_{1/2}Cu_{1/2}$)Al, ($Ni_{1/2}Mn_{1/2}$)Al, and ($Fe_{1/2}Mn_{1/2}$)Al, do not form single B2 phases at the same temperature (based on CALPHAD modeling, which have been well assessed for ternary subsystems in general). This also suggests a high-entropy effect to stabilize equimolar solid solutions in high-component-dimensional systems.

3.6. Criterion for forming single high-entropy B2 phases

Two criteria are commonly used to assess the formation of single-phase HEAs, i.e., atomic size polydispersity $\delta = 100\sqrt{\sum_{i=1}^{n} c_i\left(1 - r_i/\bar{r}\right)^2}$ and mixing enthalpy $\Delta H_{mix} = \sum_{i=1, i\neq j}^{n} c_i c_j \Omega_{ij}$, where the average atomic radius $\bar{r} = \sum_{i=1}^{n} c_i r_i$, c_i and r_i are the atomic percentage and atomic radius of the ith element, respectively. n is the number of alloying elements, and Ω_{ij} is the mixing enthalpy between i and j in the liquid phase [44]. It is proposed that the formation of a single-phase HEA solid solution is favored when $\delta \leq 6$ and -15 kJ/mol $\leq \Delta H_{\text{mix}} \leq 5$ kJ/mol. An additional indicator, VEC = $\sum_{i=1}^{n} c_i \chi_i$, where χ_i is the valence electron concentration (VEC), was introduced to predict whether an HEA forms BCC (VEC < 6.5) or FCC (VEC > 6.5) structure [45]. The corresponding values of δ, ΔH_{mix}, and VEC for seven specimens were calculated and listed in Table 1. Here, small VEC values (2.6–3.5) suggest they would favor to form BCC-like structure, but large δ values (>7 for all cases) show that they should not form HEAs of the simple BCC structure. The predictions are consistent with the experimental observations that they form BCC-based, ordered B2 phases.

The atomic size polydispersity δ calculated with 50% Al should be used to judge whether an HEA solid solution on one lattice (simple FCC or BCC) can to form. The ordered B2 HEICs are more like HECs with one element (Al in this case vs. anions in HECs) primarily occupies one sublattice and other four or five elements form a solid solution on the other sublattice. In HECs, atomic size difference of cation atoms and cation-anion bonding lengths are considered as a key parameter for predicting the formation of single HEC phases [22,23]. Here, we proposed to use atomic size polydispersity of non-Al elements, $\delta^* = 100\sqrt{\sum_{i\neq \text{Al}} c_i\left(1 - r_i/\bar{r}_{\text{non-Al}}\right)^2}$, as a refined parameter to the formation of single high-entropy B2 phases. The calculated results are listed in Table 1. It is found that the specimens #3 and #5 (single HEIC phases at 1,100 °C) as well as specimen #2 (almost single high-entropy B2 phase at 1,100 °C and true single high-entropy B2 phase at a high temperature of 1,300 °C) with $\delta^* < 1$ form single high-entropy B2 phases, thereby suggesting that δ^* could be a good indicator for forming single-phase HEICs.

A careful examination further shows that the calculated ΔH_{mix} values are in the range of −12 to −29 kJ/mol. It is interesting to note that only specimens #3 and #5 have ΔH_{mix} >−15 kJ/mol, which are the two that form single high-entropy B2 phases at 1,100 °C. For ordered B2-phase HEICs, perhaps it is more accurate to use the sum of average weighted bonding energies between non-Al and Al atoms to define a modify $\Delta H_{\text{mix}}{}^* = \sum_{i\neq \text{Al}} c_i \Omega_{\text{Al-}i}$. The calculated results are listed in Table 1. Again, only specimens #3 and #5, the two that form single high-entropy B2 phases at 1,100 °C, have the refined $\Delta H_{\text{mix}}{}^*$ >−15 kJ/mol and $\delta^* < 1$.

It is interesting to note that specimen #2 has the lowest δ^* of 0.66, but with a more negative $\Delta H_{\text{mix}}{}^*$ of −17.75 kJ/mol. Experimentally, only trace amount of secondary phase was observed in specimen #2 at 1,100 °C (Fig. 2). Moreover, it formed single high-entropy B2 phase at a higher temperature of 1,300 °C, but a secondary phase reversibly precipitated out at a lower temperature of 1,000 °C. Presumably, the negative $\Delta H_{\text{mix}}{}^*$ effect was offset by higher entropy stabilization effect at a higher temperature, which further supports that this single high-entropy B2 phase is entropy-stabilized at high temperature.

We further note that a small δ^* alone is not a good indicator for forming single-phase ternary aluminides; for example, ($Ni_{1/2}Co_{1/2}$)Al has an δ^* of ~0, but it does not form a single phase. Interestingly, current study suggests that δ^* appears to be a good indicator for forming single-phase, equimolar high-entropy aluminides of four or five components. This can be a unique "high-entropic" effect

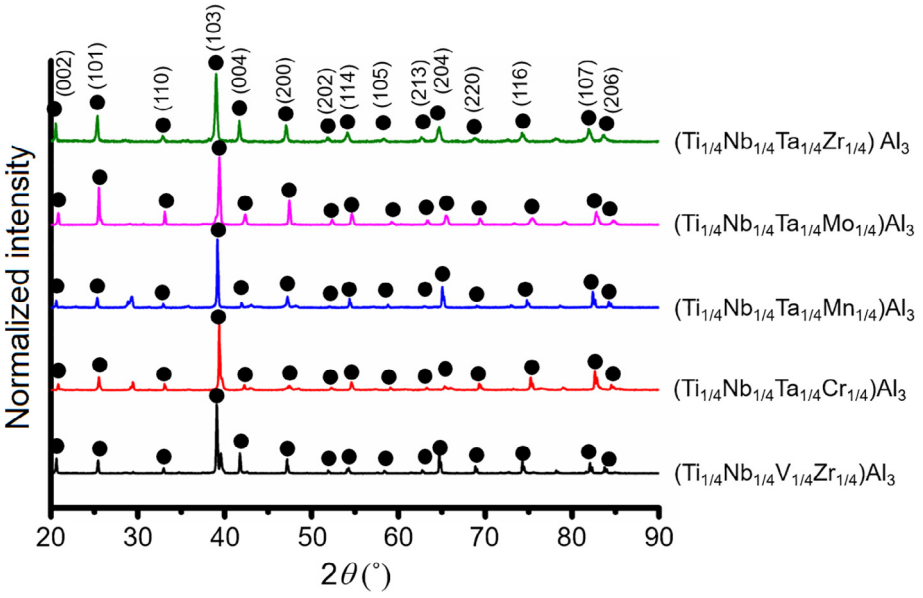

Fig. 5. (Color online) XRD patterns of five HEIC specimens with primarily the high-entropy $D0_{22}$ phase after annealing at 1300 °C for 10 h. The $D0_{22}$ phase are indexed; the unindexed peaks with low intensity correspond to the secondary phases. The high-entropy $D0_{22}$ phase dominant in all five cases (albeit some minor secondary phases).

that works only for many-component solid solutions with sufficient randomness (but not for low-order systems such as ternary alloys). It is possible that the current criterion can be extended to predict the single-phase, non-equimolar HEICs. There is also an open question on whether the proposed criterion can still be held if there are strong intermetallic former among non-Al elements. All these should be further tested with experiments.

In summary, the current results suggest that a small $\delta^*(<1)$ appears to be a good indicator to promote the formation of a single high-entropy B2 phase (and perhaps HEICs in general) of four and five components with nearly equimolar compositions, while a less negative $\Delta H_{\text{mix}}{}^*$ may help to stabilize HEICs to a lower temperature. More critical testing and possible refinement of the proposed criterion should be carried out in future studies.

3.7. High-entropy $D0_{22}$ phases

To extend the generality of this study and our discovery of single-phase HEICs, we further examined the possible formation of $D0_{22}$-phase HEICs (see Fig. 1b for the schematic structure) fabricated via the same route. We selected possible compositions based on the following principles (similar to those used for selecting possible B2-phase HEICs): (1) at least three transition metal elements are able to form equilibrium $D0_{22}$-phase binary aluminides, and (2) at least two of the $D0_{22}$-phase binary aluminides have 100% mutual solubility according to the ternary phase diagrams. Fig. 5 shows the XRD patterns of the five specimens of selected compositions: i.e., $(Ti_{1/4}Nb_{1/4}V_{1/4}Zr_{1/4})Al_3$, $(Ti_{1/4}Nb_{1/4}Ta_{1/4}Cr_{1/4})Al_3$, $(Ti_{1/4}Nb_{1/4}Ta_{1/4}Mn_{1/4})Al_3$, $(Ti_{1/4}Nb_{1/4}Ta_{1/4}Mo_{1/4})Al_3$, and $(Ti_{1/4}Nb_{1/4}Ta_{1/4}Zr_{1/4})Al_3$. All these five compositions exhibited the primary $D0_{22}$ phases after annealing at 1,300 °C for 10 h. Very few amounts of secondary phases were detected by XRD measurements. These findings further demonstrated that equimolar HEICs of mostly single high-entropy phases (albeit small amounts of secondary phases) beyond the high-entropy B2 phases can be made.

4. Conclusions

In this study, we successfully fabricated, for the first time to our knowledge, several single-phase HEICs with ordered B2 structure, in which four or five transition metal elements, e.g., Fe, Co, Ni, Mn, and Cu of equimolar fractions, occupy one sublattice, with Al on the other sublattice (albeit ~10% anti-site defects). Specifically, $(Co_{1/4}Fe_{1/4}Ni_{1/4}Mn_{1/4})Al$, $(Co_{1/4}Fe_{1/4}Ni_{1/4}Cu_{1/4})Al$, and $(Co_{1/5}Fe_{1/5}Ni_{1/5}Mn_{1/5}Cu_{1/5})Al$ can be made into single high-entropy B2 phases, while four other compositions exhibit predominantly single high-entropy B2 phases with small amounts of secondary phases. These high-entropy B2 phases are likely entropy-stabilized phases based on CALPHAD modeling and a model experiment. A new criterion for forming single high-entropy B2 phases is proposed as a new phase stability rule. Five additional HEICs of primarily $D0_{22}$ phases have been made to broaden the discovery.

The discovery of single-phase HEICs bridges the traditional metallic HEAs and emerging non-metallic HECs. Their structures are more like ionic HECs with high-entropy mixing only on one sublattice. However, comparison of experimental and calculated XRD patterns suggest the existence of ~10% anti-site defects in B2-phase HEICs (differing from most HECs with little anti-site defects). The single-phase HEICs reported in this study represents a new class of high entropy materials, which opens a new platform to explore unique mechanical, thermal, and other functional properties.

Conflict of interest

The authors declare that they have no conflict of interest.

Acknowledgments

This work was supported by a Vannevar Bush Faculty Fellowship sponsored by the Basic Research Office of the Assistant Secretary of Defense for Research and Engineering and funded by the Office of Naval Research (N00014-16-1-2569). Tao Hu acknowledges the funding support from State Key Laboratory of High Performance and Complex Manufacturing at Central South University (ZZYJKT2018-04).

Author contributions

N. Zhou conducted CALPHAD modeling and materials design. N. Zhou and T. Huang prepared specimens. S. Jiang and M. Qin conducted the characterization. T. Hu assisted the data analysis. J. Luo, T. Hu, and N. Zhou wrote the manuscript. J. Luo supervised this study. All authors discussed results, analyzed data, and reviewed the manuscript.

Appendix A. Supplementary data

Supplementary data to this article can be found online at https://doi.org/10.1016/j.scib.2019.05.007.

References

[1] Tsai MH, Yeh JW. High-entropy alloys: a critical review. Mater Res Lett 2014;2:107–23.
[2] Zhang Y, Zuo TT, Tang Z, et al. Microstructures and properties of high-entropy alloys. Prog Mater Sci 2014;61:1–93.
[3] Chou HP, Chang YS, Chen SK, et al. Microstructure, thermophysical and electrical properties in Al_xCoCrFeNi ($0 \le x \le 2$) high-entropy alloys. Mater Sci Eng B 2009;163:184–9.
[4] Senkov ON, Wilks GB, Scott JM, et al. Mechanical properties of $Nb_{25}Mo_{25}Ta_{25}W_{25}$ and $V_{20}Nb_{20}Mo_{20}Ta_{20}W_{20}$ refractory high entropy alloys. Intermetallics 2011;19:698–706.
[5] Gludovatz B, Hohenwarter A, Catoor D, et al. A fracture-resistant high-entropy alloy for cryogenic applications. Science 2014;345:1153–8.
[6] Yang T, Zhao YL, Tong Y, et al. Multicomponent intermetallic nanoparticles and superb mechanical behaviors of complex alloys. Science 2018;362:933–7.
[7] Li Z, Pradeep KG, Deng Y, et al. Metastable high-entropy dual-phase alloys overcome the strength-ductility trade-off. Nature 2016;534:227–30.
[8] Cantor B, Chang I, Knight P, et al. Microstructural development in equiatomic multicomponent alloys. Mater Sci Eng A 2004;375:213–8.
[9] Shi P, Ren W, Zheng T, et al. Enhanced strength-ductility synergy in ultrafine-grained eutectic high-entropy alloys by inheriting microstructural lamellae. Nat Commun 2019;10:489.
[10] Cai B, Liu B, Kabra S, et al. Deformation mechanisms of Mo alloyed FeCoCrNi high entropy alloy: in situ neutron diffraction. Acta Mater 2017;127:471–80.
[11] Lee C, Song G, Gao MC, et al. Lattice distortion in a strong and ductile refractory high-entropy alloy. Acta Mater 2018;160:158–72.
[12] Zhang Z, Mao MM, Wang J, et al. Nanoscale origins of the damage tolerance of the high-entropy alloy CrMnFeCoNi. Nat Commun 2015;6:10143.
[13] Kumar NAPK, Li C, Leonard KJ, et al. Microstructural stability and mechanical behavior of FeNiMnCr high entropy alloy under ion irradiation. Acta Mater 2016;113:230–44.
[14] Egami T, Guo W, Rack P, et al. Irradiation resistance of multicomponent alloys. Metal Mater Trans A 2014;45:180–3.
[15] Tang Z, Yuan T, Tsai CW, et al. Fatigue behavior of a wrought $Al_{0.5}$CoCrCuFeNi two-phase high-entropy alloy. Acta Mater 2015;99:247–58.
[16] Shi Y, Yang B, Xie X, et al. Corrosion of AlCoCrFeNi high-entropy alloys: Al-content and potential scan-rate dependent pitting behavior. Corr Sci 2017;119:33–45.
[17] Chou Y, Yeh J, Shih H. The effect of molybdenum on the corrosion behaviour of the high-entropy alloys $Co_{1.5}CrFeNi_{1.5}Ti_{0.5}Mo_x$ in aqueous environments. Corr Sci 2010;52:2571–81.
[18] Brechtl J, Chen S, Xie X, et al. Towards a greater understanding of serrated flows in an Al-containing high-entropy-based alloy. Int J Plasticity 2019;115:71–92.
[19] Niu S, Kou H, Zhang Y, et al. The characteristics of serration in $Al_{0.5}$CoCrFeNi high entropy alloy. Mater Sci Eng A 2017;702:96–103.
[20] Chen S, Li W, Xie X, et al. Nanoscale serration and creep characteristics of $Al_{0.5}$CoCrCuFeNi high-entropy alloys. J Alloys and Compd 2018;752:464–75.
[21] Rost CM, Sachet E, Borman T, et al. Entropy-stabilized oxides. Nat Commun 2015;6:8485.
[22] Gild J, Zhang Y, Harrington T, et al. High-entropy metal diborides: a new class of high-entropy materials and a new type of ultrahigh temperature ceramics. Sci Rep 2016;6:37946.

[23] Jiang S, Hu T, Gild J, et al. A new class of high-entropy perovskite oxides. Scr Mater 2018;142:116–20.
[24] Gild J, Samiee M, Braun JL, et al. High-entropy fluorite oxides. J Eur Ceram Soc 2018;38:3578–84.
[25] Sharma Y, Musico BL, Gao X, et al. Single-crystal high entropy perovskite oxide epitaxial films. Physl Rev Mater 2018;2:060404.
[26] Sarkar A, Djenadic R, Wang D, et al. Rare earth and transition metal based entropy stabilised perovskite type oxides. J Eur Ceram Soc 2018;38:2318–27.
[27] Harrington TJ, Gild J, Sarker P, et al. Phase stability and mechanical properties of novel high entropy transition metal carbides. Acta Mater 2019;166:271–80.
[28] Yan X, Constantin L, Lu Y, et al. $(Hf_{0.2}Zr_{0.2}Ta_{0.2}Nb_{0.2}Ti_{0.2})C$ high-entropy ceramics with low thermal conductivity. J Am Ceram Soc 2018;101:4486–91.
[29] Castle E, Csanádi T, Grasso S, et al. Processing and properties of high-entropy ultra-high temperature carbides. Sci Rep 2018;8:8609.
[30] Ye B, Wen T, Huang K, et al. First-principles study, fabrication and characterization of $(Hf_{0.2}Zr_{0.2}Ta_{0.2}Nb_{0.2}Ti_{0.2})C$ high entropy ceramic. J Am Ceram Soc 2019;102:4344–52.
[31] Gild J, Braun J, Kaufmann K, et al. A high-entropy silicide $(Mo_{0.2}Nb_{0.2}Ta_{0.2}Ti_{0.2}W_{0.2})Si_2$. J Materiomics 2019. https://doi.org/10.1016/j.jmat.2019.03.002.
[32] Braun JL, Rost CM, Lim M, et al. Charge-induced disorder controls the thermal conductivity of entropy-stabilized oxides. Adv Mater 2018;30:1805004.
[33] Zhang Y, Guo WM, Jiang ZB, et al. Dense high-entropy boride ceramics with ultra-high hardness. Scr Mater 2019;164:135–9.
[34] Lu Y, Dong Y, Guo S, et al. A promising new class of high-temperature alloys: eutectic high-entropy alloys. Sci Rep 2014;4:6200.
[35] Nagase T, Takemura M, Matsumuro M, et al. Solidification microstructure of $AlCoCrFeNi_{2.1}$ eutectic high entropy alloy ingots. Mater Trans 2018;59:255–64.
[36] Jiang H, Han K, Gao X, et al. A new strategy to design eutectic high-entropy alloys using simple mixture method. Mater Design 2018;142:101–5.
[37] He F, Chen D, Han B, et al. Design of $D0_{22}$ superlattice with superior strengthening effect in high entropy alloys. Acta Mater 2019;167:275–86.
[38] Zhao Y, Yang Y, Lee CH, et al. Investigation on phase stability of $Al_xCo_{0.2}Cr_{0.2}Ni_{0.2}Ti_{0.4-x}$ high entropy alloys. J Phase Equilib Diff 2018;39:610–22.
[39] Gao MC, Zhang C, Gao P, et al. Thermodynamics of concentrated solid solution alloys. Curr Opin Solid State Mater Sci 2017;21:238–51.
[40] Liu CT, George EP, Maziasz PJ, et al. Recent advances in B2 iron aluminide alloys: deformation, fracture and alloy design. Mater Sci Eng A 1998;258:84–98.
[41] Eleno L, Frisk K, Schneider A. Assessment of the Fe-Ni-Al system. Intermetallics 2006;14:1276–90.
[42] Liu XL, Lindwall G, Gheno T, et al. Thermodynamic modeling of Al-Co-Cr, Al-Co-Ni, Co-Cr-Ni ternary systems towards a description for Al-Co-Cr-Ni. Calphad 2016;52:125–42.
[43] Pike LM, Chang YA, Liu CT. Point defect concentrations and hardening in binary B2 intermetallics. Acta Mater 1997;45:3709–19.
[44] Zhang Y, Zhou YJ, Lin JP, et al. Solid-solution phase formation rules for multi-component alloys. Adv Eng Mater 2008;10:534–8.
[45] Guo S, Ng C, Lu J, et al. Effect of valence electron concentration on stability of fcc or bcc phase in high entropy alloys. J Appl Phys 2011;109:103505.

Naixie Zhou is a materials engineer at Oerlikon Metco. He obtained his Ph.D. degree in Materials Science and Engineering from the University of California, San Diego. His research interest covers computational modeling and design of high temperature materials.

Tao Hu is a professor in the School of Materials Science and Engineering at the Central South University, China. He obtained his Ph.D. degree from City University of Hong Kong in 2011. From 2011 to 2016, he did post-doctoral research in the University of California Davis and the University of California, San Diego, respectively. His research focuses on the characterization of defects in materials, e.g., grain boundaries, dislocations, precipitates, by using advanced electron microscopy. His research projects comprise oxide dispersion-strengthened (ODS) alloys, Al alloys, nanocrystalline alloys, and high entropy materials.

Jian Luo is a Professor at the University of California, San Diego. He graduated from Tsinghua University with dual Bachelor's degrees, one in Materials Science and Engineering and another in Electronics and Computer Technology. He received a M.S. degree in Materials Science and Engineering in 1999, and a Ph.D. degree in Ceramics in 2001, both from Massachusetts Institute of Technology. Prior to the current position, he was a faculty member at the Clemson University from 2003 to 2012, and a Member of Technical Staff with the Lucent Technologies and OFS from 2001 to 2003. His research group is conducting fundamental studies on solid interfaces and their roles in controlling materials fabrication and properties, flash sintering and electric effects on microstructural evolution, high-entropy ceramics and alloys, and materials for energy related applications.